Electronic Supplementary Material (ESI) for Journal of Materials Chemistry B.
This journal is © The Royal Society of Chemistry 2022

Supporting Information

Facile fabrication of biodegradable endothelium-mimicking coatings on bioabsorbable zinc-alloy stents by one-step electrophoretic deposition

Kai Pan [a], Wei Zhang [a], Hui Shi [a], Miao Dai [a], Zhenyu Yang [b], Maohua Chen [b], Wei Wei [a], Yufeng Zheng [c,], Xiaoya Liu [a,]*, Xiaojie Li [a,]**

[a] *Key Laboratory of Synthetic and Biological Colloids, Ministry of Education, School of Chemical and Material Engineering, Jiangnan University, Wuxi 214122, China*

[b] *Department of Cardiology, The Affiliated Wuxi People's Hospital of Nanjing Medical University, Jiangsu Province, Wuxi 214023, China*

[c] *State Key Laboratory for Turbulence and Complex Systems and Department of Materials Science and Engineering, College of Engineering, Peking University, Beijing 100871, China*

Corresponding authors. *Tel/fax.: (+86)510-85917763; +86-010-62767411.

E-mail address: yfzheng@pku.edu.cn (Y. Zheng); lxy@jiangnan.edu.cn (X. Liu);

xjli@jiangnan.edu.cn (X. Li)

RESULTS AND DISCUSSION

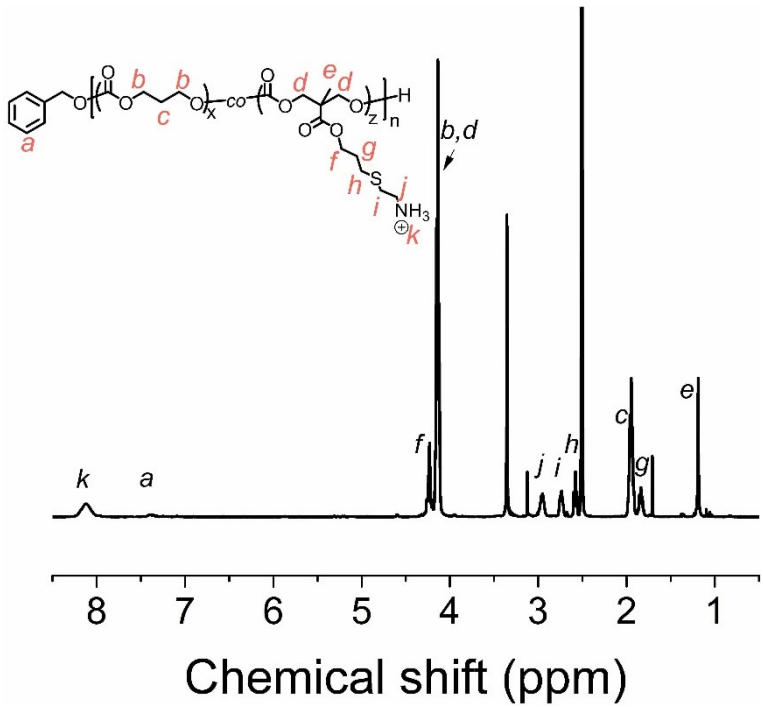

Fig. S1. ^{1}H NMR spectrum and corresponding assignment of proton signals of PMCT.

The P(MAC-CA-*co*-TMC), (PMCT) was prepared by post-polymerization modification. First, the biodegradable polycarbonate P(MAC-*co*-TMC) was synthesized according to the procedure published in our previous report[1]. Second, cysteamine hydrochloride (CA) was used to realize the amino functionalization of the polycarbonate via a subsequent free radical thiol-ene click reaction. The ^{1}H NMR spectrum and corresponding assignment for the purified product are shown in Fig. S1. The absence of the peaks of double bond at about 5.88-5.97 ppm and 5.37-5.17 ppm and the formation of new C-C bond (h, g) confirmed the successful preparation of PMCT.

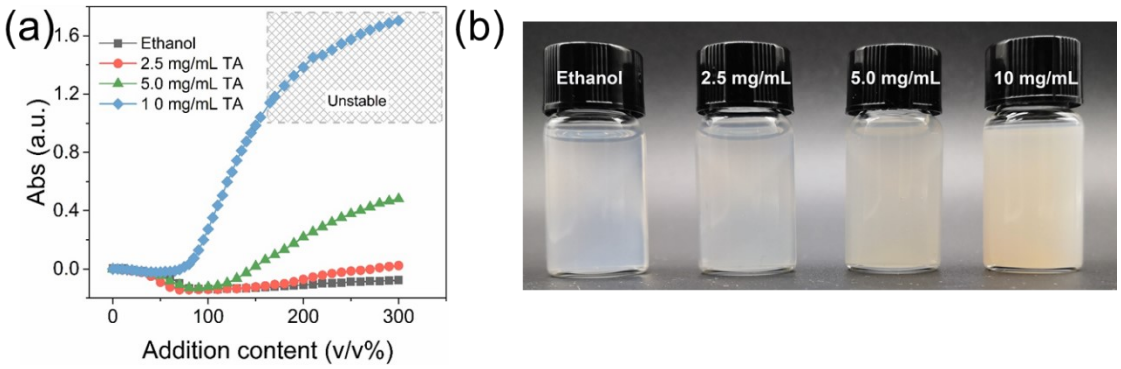

Fig. S2. (a) The self-assembly process of CP/TA monitored by real-time UV-vis spectra. (b) The corresponding digital photos of self-assembled colloidal particles.

To verify the self-assembly mechanism of colloidal particles (CP/TA). The ethanol solutions of TA with concentration of 0, 2.5, 5.0, and 10 mg/mL were separately add into methanol solution of PMCT, and the absorbance at 630 nm was monitored by UV-vis spectra (Fig. S2a). The absorbance of solution was first decrease due to the dilution effect, and then increased along with the formation of CP/TA colloidal particles which provoked the increase of turbidity. In addition, with the increase concentration of TA solution, the turbidity sharply increased at the same addition content, which indicated the hydrogen bonding and electrostatic interaction between TA and PMCT [2].

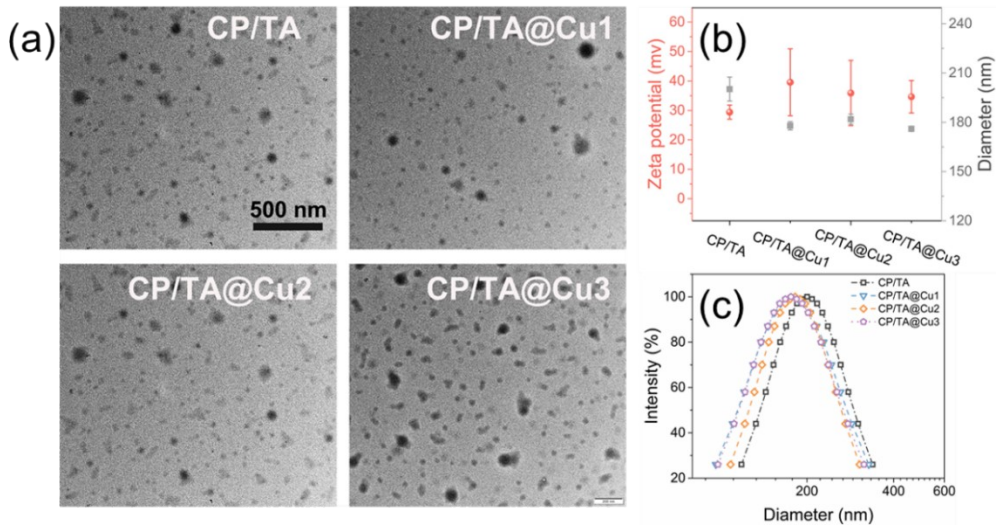

Fig. S3. Characterization of different colloidal particles: (a) TEM images, (b) average sizes and zeta potential, and (c) size distributions.

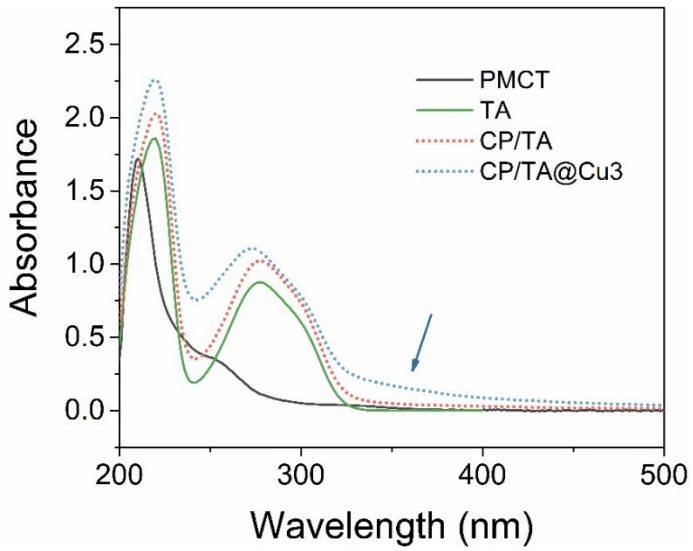

Fig. S4. UV-vis spectra of PMCT, tannic acid (TA) and colloidal particles of CP/TA and CP/TA@Cu3. (To remove the free TA and Cu^{2+} in the colloidal solution, the CP/TA and CP/TA@Cu3 colloidal particles obtained in Section 2.3 were respectively dialyzed in methanol for 5 d)

The chelation of copper ion by tannic acid unit in colloidal particles could be implied by the new formation peak at about 350 nm [3].

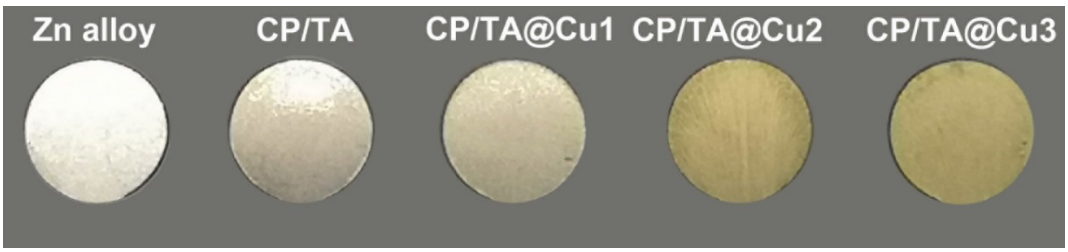

Fig. S5. The digital photos of Zn-Li alloy, CP/TA-, CP/TA@Cu1-, CP/TA@Cu2-, and CP/TA@Cu3-coated Zn alloys.

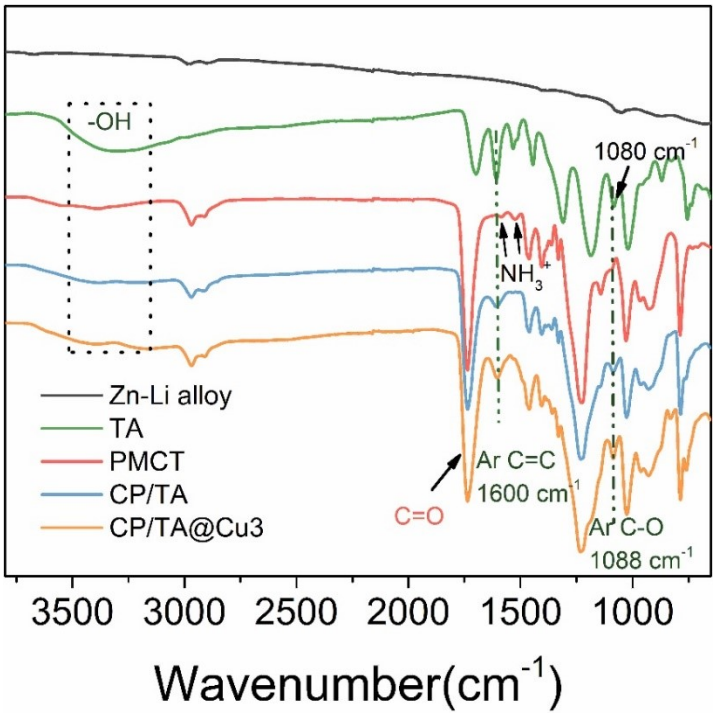

Fig. S6. The ATR-FTIR spectra of TA, PMCT, Zn-Li alloy, and two coated Zn-Li alloys (CP/TA- and CP/TA@Cu3-coated Zn alloy).

Table S1. Quantitative results of elemental XPS analysis of different samples.

Sample	C	O	N	S	Cu	Zn
Zn-Li alloy	41.77%	45.41%	--	--	--	12.81%
CP/TA	60.43%	34.46%	1.27%	3.84%	--	--
CP/TA@Cu1	61.04%	34.67%	1.00%	3.29%	0.15%	--
CP/TA@Cu2	57.51%	35.23%	2.35%	4.43%	0.46%	--
CP/TA@Cu3	60.78%	33.94%	1.14%	3.38%	0.76%	--

Table S2 Equivalent circuit parameters fitted from EIS plots.

Sample	R_s ($\Omega \cdot cm^2$)	CPE_1 ($\Omega^{-1} \cdot S^n \cdot cm^{-2}$)	n_1	CPE_2 ($\Omega^{-1} \cdot S^n \cdot cm^{-2} \cdot$)	n_2	R_c ($\Omega \cdot cm^2$)	R_{ct} ($\Omega \cdot cm^2$)
Zn-Li	42.2	1.04×10^{-4}	0.71	1.44×10^{-4}	0.80	838.9	2.01×10^{3}
CP/TA	31.3	2.03×10^{-7}	0.80	2.85×10^{-5}	0.45	1.49×10^{4}	3.22×10^{4}
CP/TA@Cu1	100.1	7.07×10^{-7}	0.79	4.68×10^{-5}	0.47	1.37×10^{4}	1.70×10^{4}
CP/TA@Cu2	100.2	5.24×10^{-7}	0.66	1.24×10^{-5}	0.61	7.39×10^{3}	1.19×10^{4}
CP/TA@Cu3	32.0	5.59×10^{-7}	0.68	1.35×10^{-5}	0.65	1.19×10^{3}	7.08×10^{3}

In the equivalent circuit model, R_s refers to solution resistance; R_c denotes the resistance of corrosion product layer or coating, which also reflects their anti-penetrating ability for the electrolyte; R_{ct} is the charge transfer resistance which reflects the difficulty of redox reactions on the Zn interface. In addition, CPE_1 and CPE_2 are constant phase elements (CPEs) related to the double-layer capacitance; the decrease of CPE often indicates enhanced corrosion resistance [3].

Table S3 Quantitative results of elemental EDS analysis for samples before immersion test.

Sample	C	O	N	S	Cu	Zn
Zn-Li	--	--	--	--	--	100%
CP/TA	55.42%	35.51%	3.89%	4.23%	0.08%	0.86%
CP/TA@Cu1	55.85%	32.2%	4.56%	5.7%	0.27%	1.43%
CP/TA@Cu2	55.18%	32.52%	4.55%	5.93%	0.49%	1.42%
CP/TA@Cu3	53.87%	32.86%	4.55%	5.84%	1.06%	1.81%

Table S4 Quantitative results of EDS analysis for samples after immersion test.

Sample	C	O	N	S	Cu	P	Zn
Zn-Li	6%	37.35%	--	0.27%	--	4.51%	51.87%
CP/TA	20.4%	37.15%	2%	5.88%	--	5.18%	29.39%
CP/TA@Cu1	51.97%	32.61%	4.58%	6.87%	0.19%	0.35%	3.43%
CP/TA@Cu2	47.41%	37.19%	5.03%	6.01%	0.45%	0.53%	3.28%

CP/TA@Cu3	47.32%	29.76%	4.02%	3.88%	0.62%	0.63%	13.76%

According previous study [4], the corrosion process of Zn-Li alloy can be explanted by steps as follows. Generally, the initial oxidation of zinc often represented by Eq (S1, S2), which can explain why the rapid increase of pH and Zn^{2+} concentrations in the initial extracts. Simultaneously, the corrosion products of ZnO and $Zn(OH)_2$ were formed by consuming the OH^- ions, as presented in Eq (S3, S4). And the Cl^- will attack the produced corrosion products (ZnO and $Zn(OH)_2$) into soluble $ZnCl_2$ as presented in Eq (S5). Afterward, the HPO_4^{2-} or HCO_3^- in the D-Hank's solution will react with Zn^{2+} and to form less soluble corrosion products, which is represented by Eq (S6, S7). Due to the polymeric coatings isolated most corrosive medium, the corrosion rate of Zn substrate was declined and above corrosion steps of coated Zn substrate was delayed, which resulted in the inhibition of pH increase and release of Zn^{2+}.

$$Zn(S) \rightarrow Zn^{2+}(aq) + 2e^- \quad \text{(S1)}$$

$$2H_2O + O_2 + 4e^- \rightarrow 4OH^- \quad \text{(S2)}$$

$$Zn^{2+} + 2OH^- \rightarrow Zn(OH)_2 \quad \text{(S3)}$$

$$Zn^{2+} + 2OH^- \rightarrow ZnO + H_2O \quad \text{(S4)}$$

$$Zn(OH)_2 + 2Cl^- \rightarrow Zn^{2+} + 2OH^- + 2Cl^- \quad \text{(S5)}$$

$$3Zn^{2+} + 2H_2PO_4^- + 4OH^- \rightarrow Zn_3(PO_4)_2 + 4H_2O \quad \text{(S6)}$$

$$5Zn^{2+} + 2HCO_3^- + 8OH^- \rightarrow Zn_5(CO_3)_2OH_6 + 2H_2O \quad \text{(S7)}$$

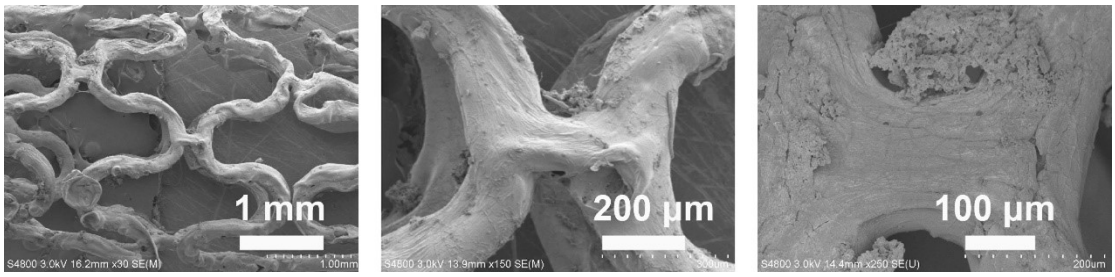

Fig. S7. SEM images of CP/TA-coated Zn-alloy stents after dynamic immersion test for 21 days.

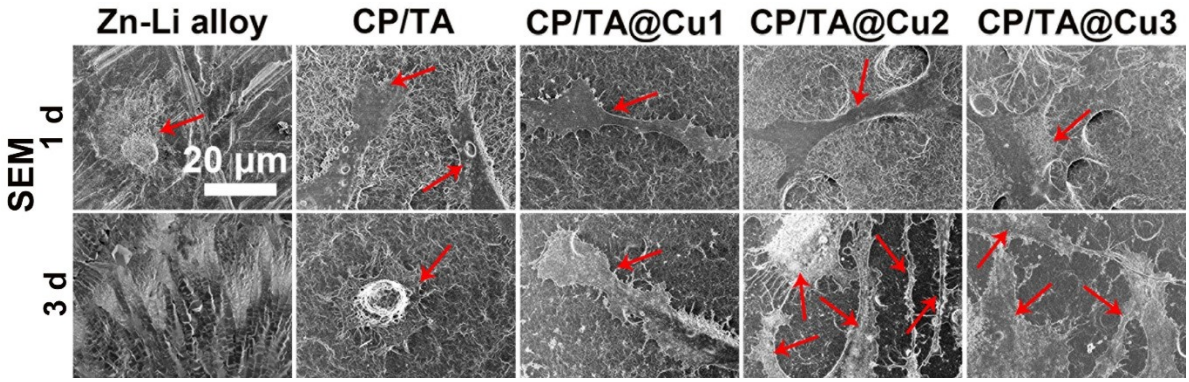

Fig. S8. Enlarged SEM images of cellular morphologies from Fig. 5a.

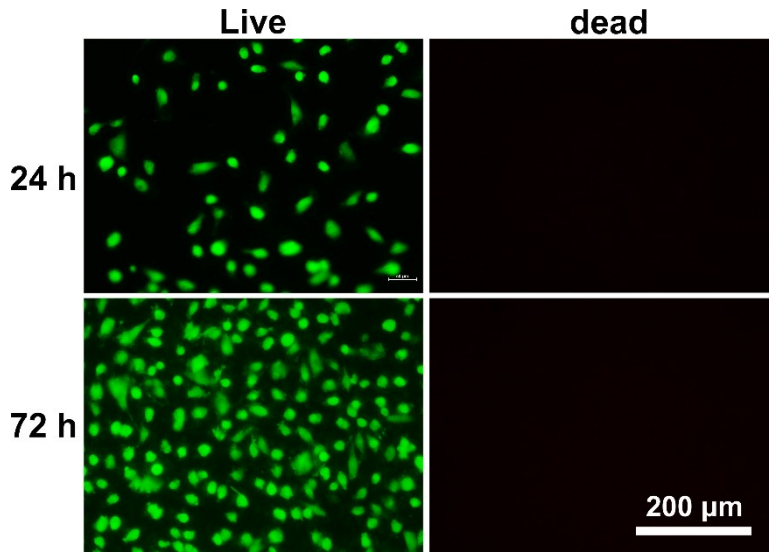

Fig. S9. Live-dead stained fluorescence images of cells on CP/TA@Cu4 (with 60 mg/mL Cu^{2+} when prepared hybrid Cu-containing colloidal particle) after culturing for 1 day and 3 days.

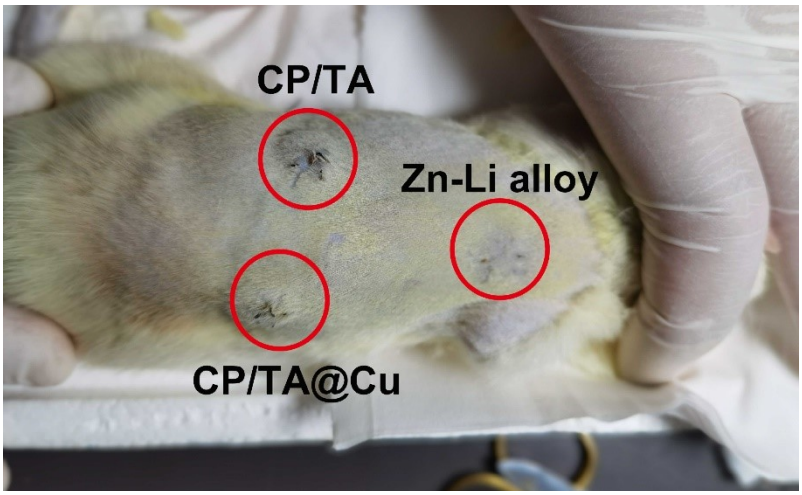

Fig. S10. The representative digital photo of the anesthesia rat after the subcutaneous implantation of bare, CP/TA- and CP/TA@Cu- coated Zn alloys.

References

(1) Pan, K.; Li, X.; Meng, L.; Hong, L.; Wei, W.; Liu, X. Photo-cross-linked polycarbonate coating with surface-erosion behavior for corrosion resistance and cytocompatibility enhancement of magnesium alloy. *ACS Appl. Bio Mater*. **2020** *3*(7), 4427-4435. https://doi.org/10.1021/acsabm.0c00411.

(2) Sun, J.; Zhu, Y.; Meng, L.; Chen, P.; Shi, T.; Liu, X.; Zheng, Y. Electrophoretic deposition of colloidal particles on Mg with cytocompatibility, antibacterial

performance, and corrosion resistance. *Acta Biomater*. **2016**, *45*, 387-398.
(3) Sheng, Y.; Yang, J.; Zhao, X.; Liu, H.; Cui, S.; Chen, L.; Zeng, R.; Wang, X.; Huang, C. H.; Li, W. Development and *in vitro* biodegradation of biomimetic zwitterionic phosphorylcholine chitosan coating on Zn1Mg Alloy. *ACS Appl. Mater. Interfaces* **2020**, *12*(49), 54445-54458.
(4) Bao, G.; Fan, Q.; Ge, D.; Wang, K.; Sun, M.; Zhang, Z.; Guo, H.; Yang, H.; He, B.; Zheng, Y. *In vitro* and *in vivo* studies to evaluate the feasibility of Zn-0.1Li and Zn-0.8Mg application in the uterine cavity microenvironment compared to pure zinc. *Acta Biomater.* 2021, *123*, 393-406.